AIMS Mathematics, 11(4): 10716–10743.
DOI: 10.3934/math.2026441
Received: 29 January 2026
Revised: 24 March 2026
Accepted: 01 April 2026
Published: 20 April 2026

http://www.aimspress.com/journal/Math

Research article

Robust dynamical behavior identification in the Rabinovich Fabrikant system using statistical measures

Haseeba Sajjad[1,2], **Adil Jhangeer**[1,3,4], **Mudassar Imran**[5,*] **and Ali R Ansari**[6]

[1] IT4Innovations, VSB-Technical University of Ostrava, Ostrava-Poruba, Czech Republic
[2] Faculty of Electrical Engineering and Science, VSB-Technical University of Ostrava, Ostrava-Poruba, Czech Republic
[3] Center for Theoretical Physics, Khazar University, 41 Mehseti Str., Baku, AZ1096, Azerbaijan
[4] Department of Computer Engineering, Biruni University, Istanbul, Turkey
[5] College of Humanities and Sciences, Ajman University, Ajman, P.O. Box 346, United Arab Emirates
[6] Centre for Applied Mathematics & Bioinformatics, Department of Mathematics and Natural Sciences, Gulf University for Science and Technology, Kuwait

* **Correspondence:** Email: Mudassar.Imran@ajman.ac.ae.

Abstract: This study presents a dynamical and statistical investigation of the Rabinovich Fabrikant system within the bounded control parameter space $(p, q) \in [-1, 1] \times [-1, 1]$, using ensembles of initial conditions sampled from $[-0.1, 0.1]$. A systematic grid-based exploration of the parameter space revealed clearly distinguishable regions corresponding to stable equilibria, sustained periodic oscillations, and unstable dynamical regimes. A grid-based systematic scan of the parameter space indicated that the space is evidently divided into easily recognizable domains that are characterized by a stable equilibrium, periodic oscillations, and unstable dynamical states. The analysis of time series and power spectral density was used to describe the time dynamics of system responses and to identify a change between steady, oscillatory, and broadband states of the system. In addition to these classical dynamical diagnostics, an ensemble-based statistical analysis was carried out to measure the variability of the system dynamics. The probability distributions of the dynamical states were measured by kernel density estimation, which demonstrated that stable and periodic regimes have convergent and sharp distributions, and transitional regions have wider distributions and slower convergence. Moreover, empirical cumulative distribution functions will gave more information about the structure and variability of the distribution of the system responses in various parameter regimes. Sensitivity analysis also implied that the impact of initial conditions is also highly parameter sensitive and is especially pronounced at regime boundaries. These findings offer a quantitative and reproducible parameter space mapping of the dynamics of RF systems and make ensemble-based

statistical diagnostics fundamental instruments to measuring robustness and uncertainty in nonlinear chaotic systems.

Keywords: nonlinear dynamical systems; statistical analysis; power spectral density; kernel density estimation; empirical cumulative distribution function; ensemble sensitivity; parametric space analysis
Mathematics Subject Classification: 37M05, 37M10, 62G07

1. Introduction

Nonlinear dynamical systems provide a fundamental framework for modeling complex time-dependent phenomena in physics and engineering, where nonlinear interactions can produce behaviors such as multistability, oscillations, and chaos [1]. They are nonlinear systems in the sense that their laws of evolution involve nonlinear functions of the state, capable of giving rise to behaviors that cannot occur in purely linear systems, such as multiple equilibrium, self-sustained oscillations, quasi-periodicity, and chaos [2]. This is an expressive power that makes nonlinear dynamics essential in the real-world to capture realistic behavior, but it also has mathematical and computational challenges that are still an active research topic [3].

The Rabinovich Fabrikant (RF) system is highly sensitive to changes in the control parameters and initial conditions. Minor changes of the parameters can lead to changes in the states of stable equilibria, periodic oscillations, and unstable dynamical regimes because of the complicated system of parameter space [4]. Similarly, in a multistable system, small changes in the initial condition have the ability to cause trajectories to cross into other sets of attractors and have different long-term behavior under the same parameter conditions [5]. Its practical implications in engineering and the applied sciences are both to make design and control more complex, to provide opportunities to ensure communication security, and to improve signals and power harvesting in cases where chaos is used well [6].

Grzegorz Litak [7] investigated chaotic vibrations in a regenerative cutting process using a nonlinear model of one degree of freedom. The study showed that the nonlinear interaction between the cutting tool and the workpiece can generate periodic, quasi-periodic, and chaotic chatter vibrations depending on the system parameters. Watanabe et al. [8] developed a nonlinear jump car model to analyze vibration dynamics of off-road vehicles. Their results demonstrated that delayed feedback active suspension control can effectively suppress chaotic vibrations and improve vehicle stability in rough road conditions. D. Feng proposed a compactor–soil coupling model that incorporates mechanical inertia to better capture nonlinear dynamic responses in compaction systems [9]. The study also applied delayed feedback active suspension control, which significantly reduced oscillations and improved vibration isolation performance.

Nonlinear dynamical models are important for various engineering and scientific applications, including vibration analysis, secure communications, and signal processing [10]. Some of the subsystems of the natural sciences encompass nonlinear models of interactions within a population, neuronal networks, the working of the heart, pattern formation, and climate [11]. In all these fields, long-term behavior stability and quantitative characterization are required in the design of interventions, determining risk, and understanding the observed data [12].

The practical relevance of nonlinear dynamical systems and chaotic attractors is justified by their

application in a wide variety of fields [13]. As an example, chaotic-based models have been extensively applied to secure-communication systems [14] to provide a high level of encryption and data security through chaotic synchronization processes. Nonlinear dynamical models are also important in vibration control and energy harvesting systems, where the question of nonlinear oscillations can be used to damp unwanted vibrations in engineering structures [15]. A parametric space categorization is a statistical analysis method of a parameter domain that divides it into a grid, and then the system is simulated under many initial conditions to gather simple numerical characteristics, such as maximum amplitude, long-term averages, or measures of energy [16]. The values of these indicators are subsequently statistically analyzed to classify the dynamic regimes associated with parameter values, typically differentiating among stable, oscillatory, and divergent behaviors [17].

The RF system is a three-dimensional nonlinear dynamical system that was proposed to describe how high-frequency electromagnetic waves and low-frequency plasma oscillations interact. It is also famous for having rich and complex dynamics and multistability, chaotic and hyperchaotic attractors, hidden attractors, and extreme parameter and initial condition sensitivity. The popularity of RF systems allows them to be as benchmark models in nonlinear dynamics and chaos theory. Due to these properties, RF systems have been applied in the fields of plasma physics, nonlinear signal processing, secure communications, chaos-based encryption, and the study of extreme events in complex systems [18].

Further studies investigated the dynamics and multistability of the RF system, which turned out to be transient, with two or more attractors existing at the same parameter values, and the system dynamics being highly sensitive to initial conditions [19]. Lyapunov-based analysis and dynamic regime maps have been used systematically in defining periodic, quasi-periodic, and chaos regimes across parameter planes [20].

Danca et al. [21] explored the strange dynamical behavior of the system and showed that there are concealed attractors to the system in both numerical simulations and phase-space analysis. Their analysis aims primarily at distinguishing complex attractor structures and providing a description of the variety of dynamical behavior in the RF system. The RF system may exhibit a long-lived transient chaotic attractor that exists for a long time but has a finite period, after which the trajectories converge to stable states. Danca [22] observed that these hidden attractors arise from the complex organization of the phase space within the system. This observation highlights how the dynamics of the RF system are sensitive to initial conditions and variations in parameters. Kuznetsov and Turukina [23] applied bifurcation analysis and Lyapunov-based diagnostics to the system to gain insight into the periodic and chaotic changes of the system. They mainly do deterministic dynamical analysis rather than statistical characterization of system variability.

The RF system has been demonstrated to have some hidden strange nonchaotic attractors, in which attractors that had previously been referred to as chaotic actually are fractal sets and have aperiodic dynamics and negative finite-time Lyapunov exponents. In this study, to separate these attractors between classical chaotic and quasiperiodic attractors, finite-time Lyapunov exponents, the 0-1 test, power spectral density, and recurrence plots are used, thus extending the knowledge of the complicated attractor topography of the system [24]. A more recent paper [25] generalized the classical three-dimensional RF system to a four-dimensional continuous time dynamical system through the augmentation of the state. The resultant system showed hyperchaotic behavior with coexistence attractors, where the Lyapunov exponents and multistability were examined using bifurcation and

waveform analysis. Adaptive control and synchronization were also used to stabilize the chaos.

Recent research highlights the possible absence of reliability of single-trajectory analysis in the expression of stability in nonlinear systems and highlights the application of ensemble-based and probabilistic metrics in the determination of statistically significant system behavior. An example of this was found by Alvares et al. [26], who presented a distance-based probabilistic quantity stabilizer to define the resilience of an attractor to finite perturbations, using ensemble-style arguments to achieve stability under more than one starting point. An ensemble-localized kernel density estimation-based method was found to be bias motivated by ensemble representations, as discussed in Popov et al. [27]. The analysis of fine-scale distributional quantities was designed to achieve better density estimates and practicality in cases in which the underlying distribution is intricate. The method helps to understand the type of distributional analysis one undertakes by estimating a probability density function of variables derived with observable high-dimensional initial conditions being run by large-scale missionaries.

Feudel explored the phenomenon of multistability in nonlinear systems, demonstrating that a single parameter set can support multiple coexisting attractors where the final state is determined entirely by the basin of attraction of the initial conditions [28]. This reality necessitates a shift from local eigenvalue analysis to global probabilistic stability measures. Addressing this need, Menck et al. introduced basin stability as a method to quantify attractor robustness against large perturbations [29], a concept Brzeski et al. later applied to mechanical oscillators to estimate the statistical probability of safe versus unsafe outcomes [30]. Collectively, these works argue that for complex or delayed networks, stability must be understood as a measure of state-space volume rather than only local convergence.

Anishchenko et al. argued that the statistical properties of dynamical systems, specifically the approximation of invariant measures, provide a more robust framework for stability analysis than individual trajectories in chaotic regimes [31]. This statistical perspective was extended by Galatolo et al., who evaluated the temporal consistency of numerical schemes in approximating long-term behavior [32], and by Baladi, who utilized transfer operators and Sinai–Ruelle–Bowen (SRB) measures to define chaotic dynamics via correlation decay and distribution-level descriptors [33].

In addition to these theoretical models, Varga et al. showed that dissipation in physical frameworks can create complex "shrimp-shaped" periodic windows within the range of parameters [34]. Similar structures were observed in the parameter space of the Ikeda map, where color-coded bifurcation diagrams revealed regions of periodic and chaotic behavior, specifically identifying complex "shrimp-like" structures [35].

Although the RF system has been extensively studied using traditional nonlinear dynamical analysis methods such as time-series analysis, bifurcation diagrams, and spectral techniques, the existing literature primarily focuses on deterministic characterizations of system behavior. Most past studies utilized a limited set of methods, analyzing the system dynamics at a single parameter point or through discrete parameter sweeps, as illustrated in Table 1. Consequently, the overall dynamical structure and statistical variability of the system have not been thoroughly examined. In particular, there has been a lack of systematic statistical characterization of the parameter space and a limited exploration of the variability of trajectories using ensemble-based studies. To address this gap, the current work integrates deterministic dynamical diagnostics such as time-series analysis and power spectral density with statistical techniques, including kernel density estimation and empirical cumulative distribution

functions. This integrated framework enables a comprehensive statistical exploration of the RF system, providing a quantitative account of its variability, sensitivity to initial conditions, and distributional characteristics of dynamical responses across the parameter space. Figure 1 shows the graphical abstract, providing a visual summary of the study.

The remainder of this paper will be structured as follows. Section 2 presents the preliminaries and methodological framework applied in this study, including time-series analysis, power spectral density estimation, parameter-space categorization, kernel density estimation, and empirical cumulative distribution functions. The dynamical analysis is presented in Section 3 in which the response of the system is studied in terms of time-series representation and power spectral analysis. Section 4 provides a statistical analysis of system behavior, categorizing parameter space, and ensemble-based analysis, such as using kernel density estimation and empirical cumulative distribution functions.

Table 1. Comparison of analytical techniques employed in previous studies and the present work.

Ref.	Time-Series Analysis	Power Spectral Density	Parameter Space Map	Ensemble Analysis	Kernel Density Estimation	Cumulative Distribution Function
[7]	✓	×	×	×	×	×
[8]	✓	×	×	×	×	×
[9]	✓	×	×	×	×	×
[19]	✓	×	✓	×	×	×
[20]	✓	×	✓	×	×	×
[21]	✓	×	×	×	×	×
[22]	✓	×	×	×	×	×
[23]	✓	×	✓	×	×	×
[24]	✓	✓	×	×	×	×
[25]	✓	×	×	×	×	×
[26]	×	×	×	✓	×	×
[27]	×	×	×	✓	✓	×
[28]	×	×	×	✓	×	×
[29]	×	×	×	✓	×	×
[30]	×	×	×	✓	×	×
[31]	×	×	×	✓	×	×
[32]	✓	×	×	✓	×	×
[33]	×	×	×	✓	×	×
[34]	×	×	✓	×	×	×
[35]	×	×	✓	×	×	×
Present Work	✓	✓	✓	✓	✓	✓

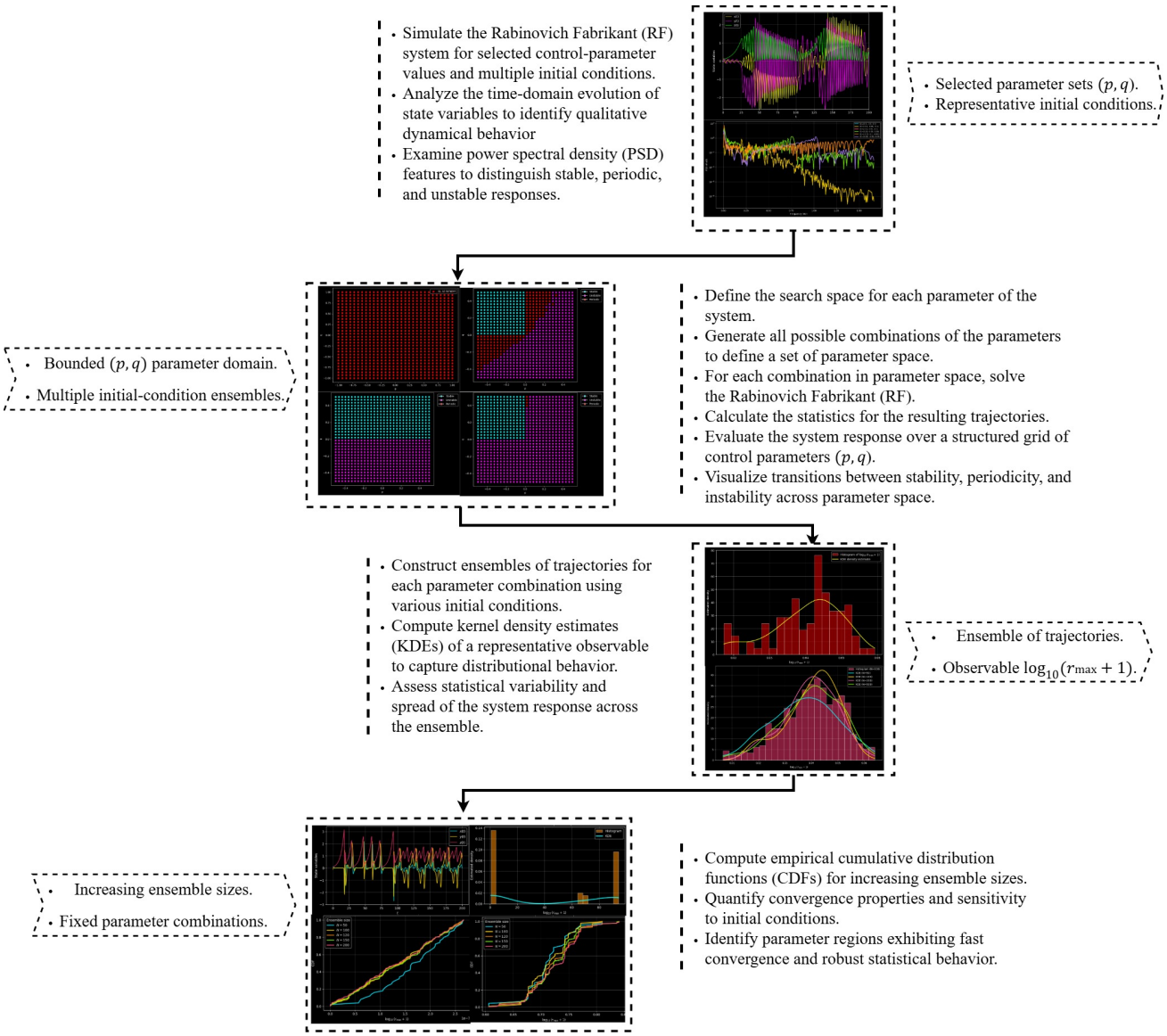

Figure 1. Graphical abstract of parameter-space exploration and sensitivity analysis.

2. Preliminaries

In order to explore the dynamical behavior and statistical analysis across parameter variation, we consider a three-dimensional nonlinear model. It is a highly nonlinear system with rich behavior and, thus, it is an appropriate representative test case. In this work, we consider a modified RF system [36]. The equations of the dynamics are the following nonlinear ordinary differential equations:

$$\begin{cases} x'(t) = y(t)\,(z(t) - 1 + x(t)^2) + p\,x(t), \\ y'(t) = x(t)\,(3z(t) + 1 - x(t)^2) + p\,y(t), \\ z'(t) = -2\,z(t)\,(q + x(t)\,y(t)), \end{cases} \tag{2.1}$$

where $x'(t)$, $y'(t)$, and $z'(t)$ denote the time derivatives of $x(t)$, $y(t)$, and $z(t)$, respectively. The state of the system is represented by the variables x, y, and z, and the main control parameters are p and q. The first two equations contain the linear parameter p as px and py.

- At $p < 0$, the terms behave as linear damping of x and y, causing them to tend to shrink.
- At $p > 0$, they behave like linear excitation or gain, and tend to amplify the amplitudes.
- The system can be moved between different stability regimes by varying p. Therefore, p is an effective damping (or gain) coefficient of the x and y components and is a bifurcation parameter governing the stability of the components.

The parameter q is present in the third equation under the factor $q + xy$, which is multiplied by z.

- When xy is small, then the sign of q will decide whether z tends to grow ($q > 0$) or decay ($q < 0$).
- Here, q is a growth or decay coefficient of the dynamics of z and is, therefore, a coupling and bifurcation parameter.

In the numerical exploration of the RF system (2.1), we limit ourselves to a finite set of parameter space and to utilize initial conditions. In this work, the ranges of the control parameters and initial conditions taken are shown in Table 2.

Table 2. Parameter and initial-condition ranges used in this study.

Quantity	Symbol	Range / Value
Control parameter	p	$[-1, 1]$
Control parameter	q	$[-1, 1]$
Initial state	$x(0)$	$[-0.1, 0.1]$
Initial state	$y(0)$	$[-0.1, 0.1]$
Initial state	$z(0)$	$[-0.1, 0.1]$

In order to examine the dynamical properties of system (2.1), several analytical methods are used. The primary analytical techniques that aid in describing time-domain dynamics, frequency-domain features, parameter-based regimes, and ensemble statistical behavior are discussed. Collectively, these methods provide a robust and objective explanation of the dynamics of the system that goes beyond the description of individual routes.

2.1. Time series

In this study, time-series analysis [37, 38] is utilized to examine the variations in the state variables of the RF system, represented as $x(t)$, $y(t)$, and $z(t)$. Numerical integration of the governing equations is performed to compute the trajectories, which are subsequently analyzed to identify transient behavior, periodic oscillations, and irregular dynamics. The identification of stable, oscillatory, and irregular regimes is conducted visually using time-series plots, before performing statistical analysis of the trajectories.

2.2. Power spectral analysis

The power spectral density (PSD) of the state variables is calculated using the Welch method [39] to identify the most important periodic oscillation frequencies and broadband spectral properties due to periodic and chaotic dynamics. The PSD of a time-dependent signal $x(t)$ is defined as:

$$S_x(f) = \lim_{T\to\infty} \frac{1}{T} \left| \int_0^T x(t)\, e^{-2\pi i f t}\, \mathrm{d}t \right|^2 . \tag{2.2}$$

In numerical computations, PSD is estimated using the Welch method as:

$$\hat{S}_x(f) = \frac{1}{K} \sum_{k=1}^{K} S_x^{(k)}(f). \tag{2.3}$$

2.3. Systematic parametric space categorization

To investigate the global dynamics of the RF system, a systematic exploration of the (p, q) parameter space is performed. The parameter plane is then sampled in a dense grid and the differential equations defining the system are numerically integrated to obtain the system trajectories corresponding to each pair of parameters. The dynamical behavior is measured by statistical measures of the simulated trajectories instead of merely using visual examination of phase portraits or time-series plots to determine the dynamical behavior. In particular, the variability of each state variable is determined by calculating the maximum and minimum values that it attains during the numerical integration period. These quantities give some idea about the amplitude of movement of the system states, and they can be used to compare the dynamical responses of different combinations of parameters. The consistent classification of the behavior of the system in the full parameter plane (p, q) is achieved by applying the same statistical criterion to all the points of the parameters and the starting conditions. With the state variable $x(t)$ of the problem, the maximum and minimum values in the region of integration are defined as follows:

$$X_{\max} = \max_t x(t), \qquad X_{\min} = \min_t x(t),$$

and similarly for $Y_{\max}, Y_{\min}$ and $Z_{\max}, Z_{\min}$. The variation (or range) of each component is then defined as:

$$\Delta X = X_{\max} - X_{\min}, \qquad \Delta Y = Y_{\max} - Y_{\min}, \qquad \Delta Z = Z_{\max} - Z_{\min}.$$

From these three quantities, one overall measure of the total variation of the system is obtained as:

$$\Delta_{\text{overall}} = \max\{\Delta X,\, \Delta Y,\, \Delta Z\}.$$

This has the greatest amplitude of movement of any of the variables and is the statistical measure of behavior categorization.

2.4. Kernel density estimation

The kernel density estimation (KDE) [40, 41] is used to estimate the probability density of scalar observables obtained from numerical simulations of the RF system. In this study, KDE is used on collections of trajectories starting at various initial conditions and parameter values. In each simulation,

the scalar values generated through the time series are assembled and applied in the development of empirical probability density distributions that describe the statistical variability of the system dynamics.

The dynamical system is numerically simulated in ensembles of initial conditions that are randomly chosen in a limited region of the phase space. For each fixed pair of control parameters (p, q), multiple trajectories are computed, and the resulting scalar observables are statistically measured using KDE. This ensemble method gives the variability of the system response produced by variations in the initial conditions to be characterized.

To obtain the instant radial distance of the origin of each numerical trajectory, the radial distance is calculated as:

$$r(t) = \sqrt{x(t)^2 + y(t)^2 + z(t)^2}.$$

The optimum achieved during the integration period is given as

$$r_{\max} = \max_t r(t).$$

This is a scalar measure of the largest excursion of the trajectory in the phase space and the overall effect of all state variables. Table 3 shows a summary of typical physical applications of KDE.

Table 3. Physical applications of KDE for analyzing distributions of observables in dynamical and complex systems.

Field	Typical observable	Physical interpretation
Nonlinear dynamics	Peak amplitude, return times, $r_{\max}$	Estimates the distribution of trajectory-based measures to quantify variability, multistability, and sensitivity to initial conditions.
Fluid dynamics	Velocity increments, vorticity, energy dissipation	Approximates probability density functions of intermittent quantities and reveals heavy tails associated with extreme events.
Plasma physics	Fluctuation amplitudes, transport bursts	Identifies non-Gaussian distributions and bursty transport statistics from time-series measurements or simulations.
Climate and geophysics	Temperature anomalies, precipitation extremes	Estimates probability densities and tail behavior to study variability and extreme-event likelihood.
Statistical mechanics	Energy, magnetization, order parameters	Constructs empirical distributions to characterize phase transitions and fluctuations in microscopic or coarse-grained variables.
Signal processing	Noise amplitude, spectral features	Provides smooth density estimates for noisy measurements to identify regimes, modes, or transitions in experimental data.

2.5. Empirical cumulative distribution functions

To statistically analyze the variability of the response of the system between different sets of initial conditions, empirical cumulative distribution functions (CDFs) are calculated for the quantity [42,43]:

$$\log_{10}(r_{\max} + 1),$$

where $r_{\max}$ represents the farthest radial distance reached by a trajectory during the time interval used in integration in the absence of transients. A set of initial conditions is created in the chosen state space region in each pair of parameter values (p, q). The numerical integration of the resulting trajectories is performed and the relevant values of $r_{\max}$ are accumulated to form empirical CDFs.

3. Dynamical simulations of the RF system

This section provides insight into the underlying dynamical behavior of the RF system through the character of its response under various initial conditions. This section analyzes the time-series development of the system states to elicit both time patterns and transitions of the system, and uses power spectral analysis to detect dominant frequencies, providing a complete explanation of periodic behavior and spectral properties.

3.1. Time series characterization of dynamical behavior

This section presents the time series study of the RF system to observe time behavior and also identify how varying parameters can change stability and long-term dynamics. The time series dynamics of the RF system are plotted in Figures 2–4 under various initial conditions and parameter values showing how parameter variation affects the qualitative behavior, stability, and long-term behavior of the system. Table 4 is a summary of the combinations chosen for the control parameters (p, q) and initial conditions to study the time-series dynamics of the system with the different cases.

Table 4. Time-series analysis for different cases.

Cases	p	q	Initial Conditions
Case 1	−0.05	0.05	(0.10, −0.10, 0.10)
Case 2	−0.25	−0.10	(0.10, −0.10, 0.10)
Case 3	−0.05	0.15	(−0.10, −0.05, −0.10)
Case 4	0.00	0.45	(−0.10, −0.05, −0.10)
Case 5	−0.10	0.20	(−0.10, 0.05, −0.10)
Case 6	−0.05	0.40	(−0.10, 0.05, −0.10)

Figure 2(a) shows the time dependence of the state variables $x(t)$, $y(t)$, and $z(t)$ with the parameter values $p = -0.05$, $q = 0.05$. The time series signals are sustained and have high levels of oscillation, as the amplitudes vary considerably during the simulation. Even though the trajectories are contained in a finite area in the state space, they are not drawn to a fixed equilibrium or to some simple periodic orbit. This outcome is an indication that the system dynamics are sensitive to internal coupling with the specified parameter configuration.

The time series of the state variables $x(t)$, $y(t)$, and $z(t)$ when $p = -0.25$, $q = -0.10$ is illustrated in Figure 2(b). The system has a transient response at the beginning of the adjustment conditions to the prescribed initial conditions. Following this temporary period, the trajectories become stable in oscillatory movement with almost constant amplitude. This phenomenon implies that the nonlinear interactions present in the system are balanced by the effects that depend on the parameters, and as a result, the system can sustain constant oscillations over time.

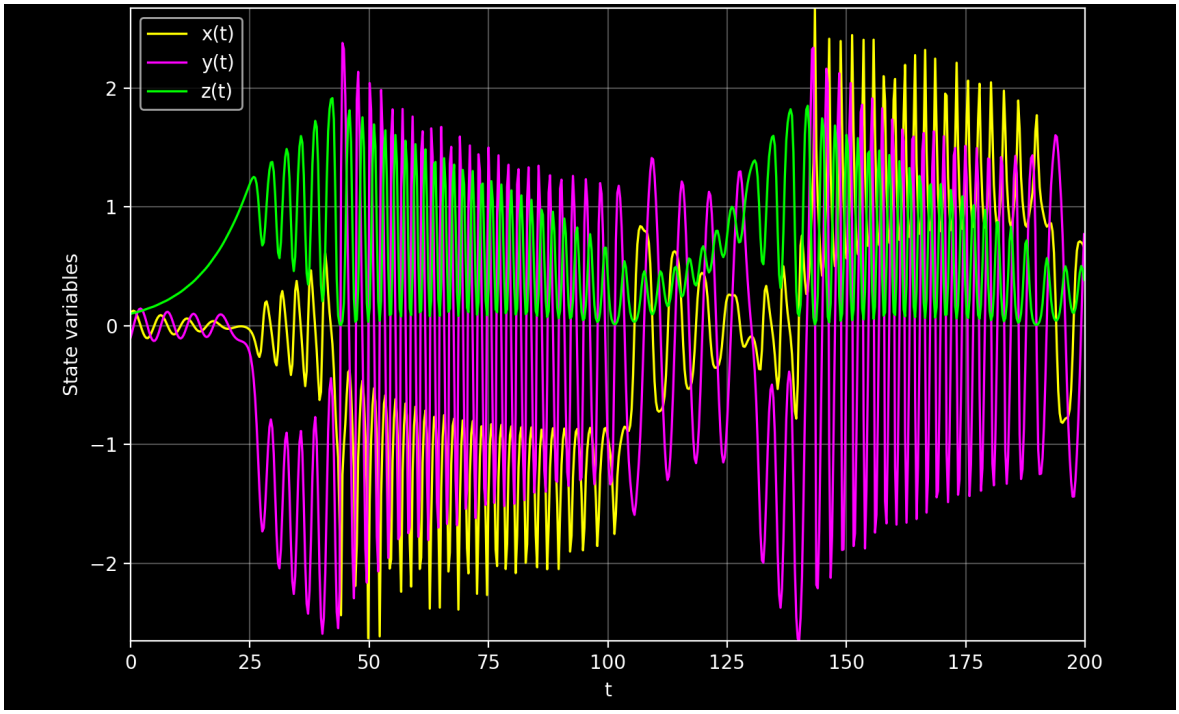

(a) $p = -0.05$, $q = 0.05$

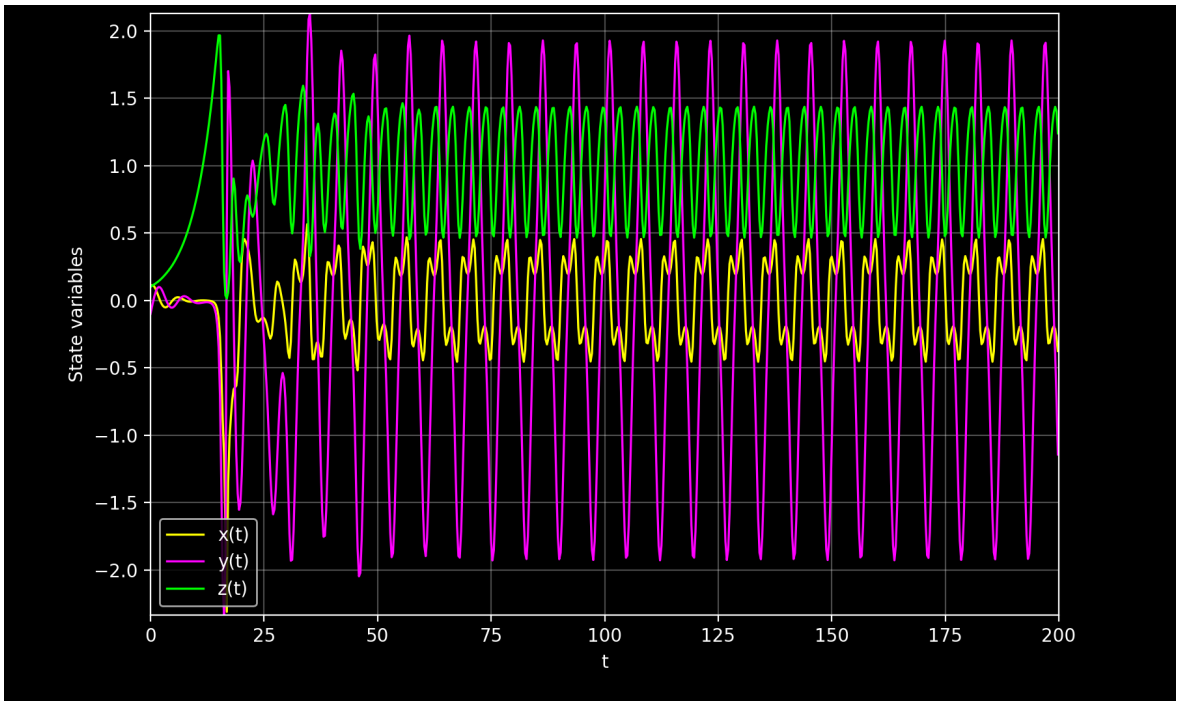

(b) $p = -0.25$, $q = -0.10$

Figure 2. Time-series plots of state variables $x(t)$, $y(t)$, and $z(t)$ for two sets of parameters with initial conditions $(0.10, -0.10, 0.10)$.

The system time domain behavior at $p = -0.05$, $q = 0.15$ is shown in Figure 3(a) through the

evolution of $x(t)$, $y(t)$, and $z(t)$ with the starting values $(-0.10, -0.05, -0.10)$. The trajectories are oscillatory in the first phase of the evolution at fixed amplitude, which decreases as time progresses. This decrease in amplitude of the oscillations means that there is some damping in the dynamics of the system. Over time, all state variables decrease to zero, which indicates a convergence to an equilibrium point.

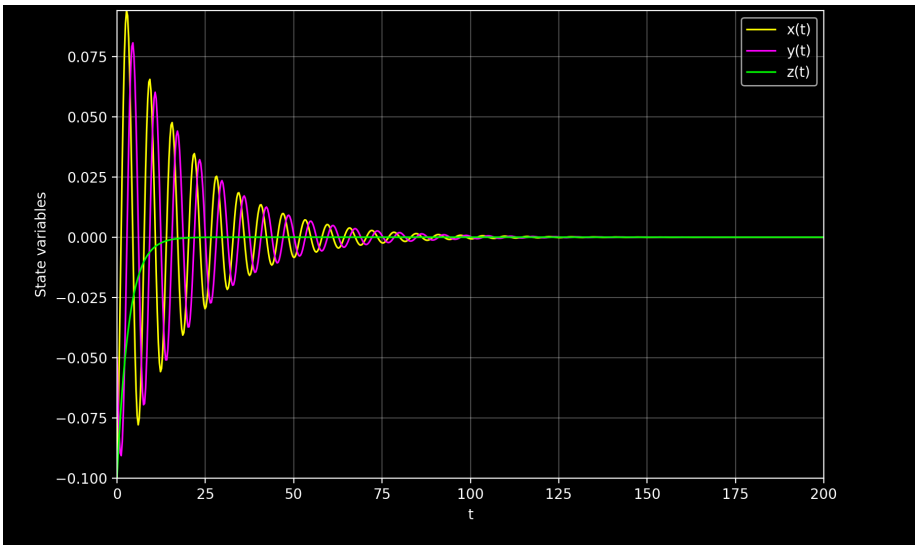

(a) For $p = -0.05$, $q = 0.15$

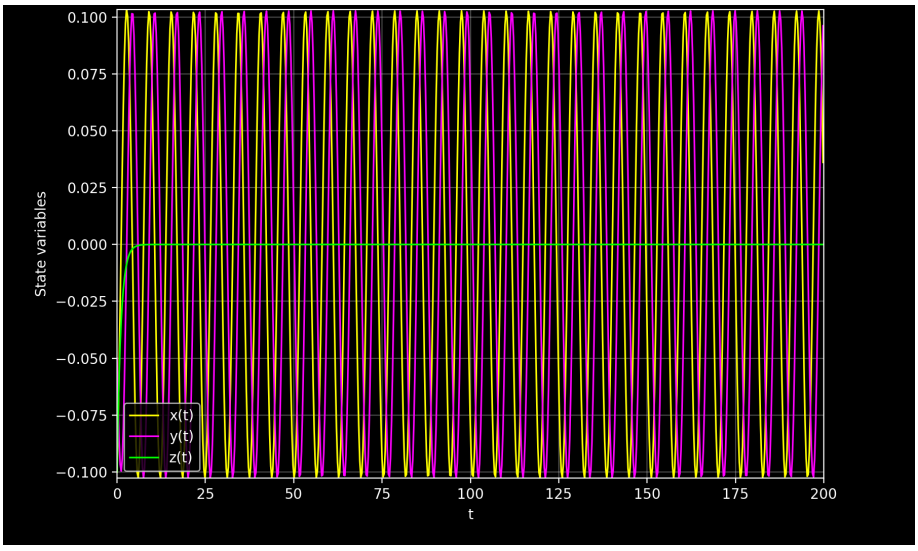

(b) For $p = 0.00$, $q = 0.45$

Figure 3. Time-series plots of state variables $x(t)$, $y(t)$, and $z(t)$ for two sets of parameters with initial conditions $(-0.10, -0.05, -0.10)$.

To further illustrate this behavior, 3(b) shows the time series behavior of the state variables under the same parameter values of $p = 0.00$, $q = 0.45$ with the initial conditions $(-0.10, -0.05, -0.10)$. There is a short transient time followed by sustained oscillations of almost constant amplitude throughout the time interval. The oscillatory motion is confined and periodic, which signifies the existence of

a periodic dynamical regime. The persistence of periodic motion over a long period indicates the importance of parameter values in ensuring the incidence of constant energy exchange between the state variables.

Figure 4(a) illustrates the dynamics of the time series of the state variables at the parameter values $p = -0.10$, $q = 0.20$ with the initial conditions $(-0.10, 0.05, -0.10)$. At the onset of the evolution, the system can be described as oscillatory with fairly high amplitudes. The oscillations gradually diminish and eventually disappear, with all of the variables going to zero. Such convergence makes one think that the system moves toward an equilibrium point. In addition, the time series behavior of the state variables for $p = -0.05$, $q = 0.40$ with the same initial conditions $(-0.10, 0.05, -0.10)$ is shown in Figure 4(b). In the long-run, the oscillations eventually tend to zero, and the state variables approach zero. The long-term behavior indicates that the equilibrium point is steady with this parameter set-up. The time series responses verify the fact that the system relaxes to a steady state following transient dynamics.

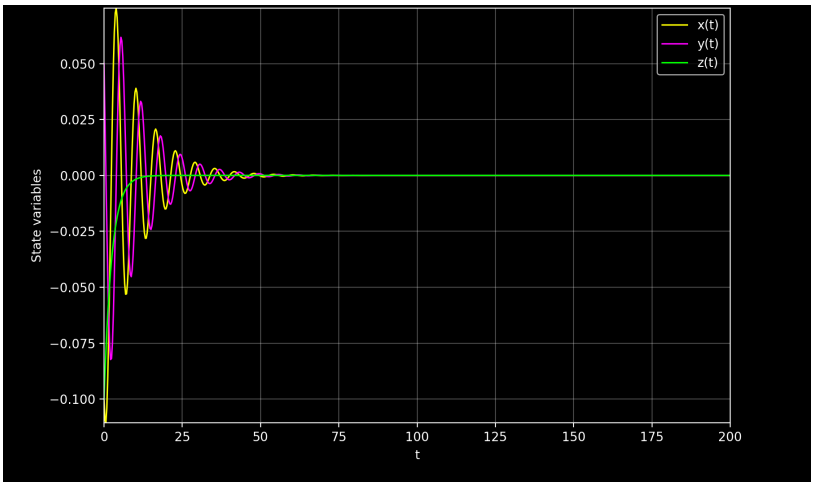

(a) For $p = -0.10$, $q = 0.20$

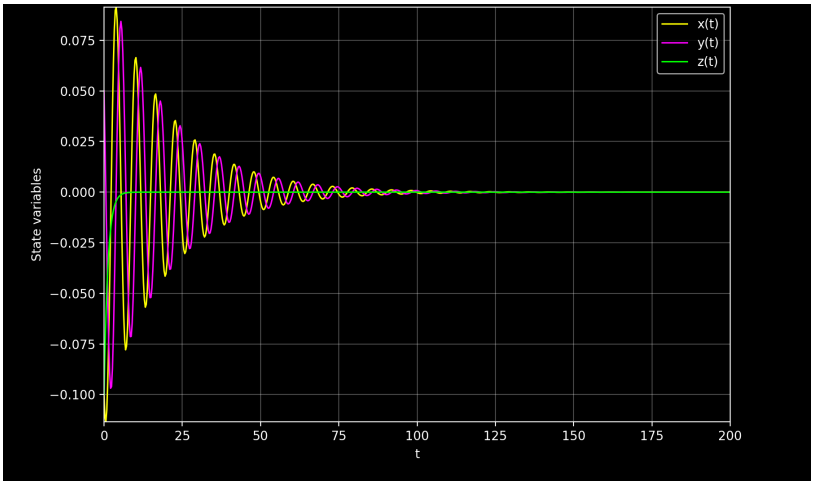

(b) For $p = -0.05$, $q = 0.40$

Figure 4. Time-series plots of state variables $x(t)$, $y(t)$, and $z(t)$ for two sets of parameters with initial conditions $(-0.10, 0.05, -0.10)$.

3.2. *Power spectral analysis of the system response*

In this section, PSD analysis is adopted to characterize the RF system, oscillatory behavior, and frequency content due to the change in initial conditions. Figure 5 shows the spectral analysis of the power of the state variable $x(t)$ for multiple initial conditions. The PSD of the state variable $x(t)$ is calculated using the Welch method and with a fixed number of parameters, and several curves are drawn, each representing different initial conditions, as shown in Figure 5(a). The spectrum is distinguished by a high weight of low frequencies and a monotonic and smooth decrease in power with frequency. The fact that sharp spectral peaks are absent means that the system dynamics in this regime are controlled by slow temporal variations as opposed to sustained periodic oscillations.

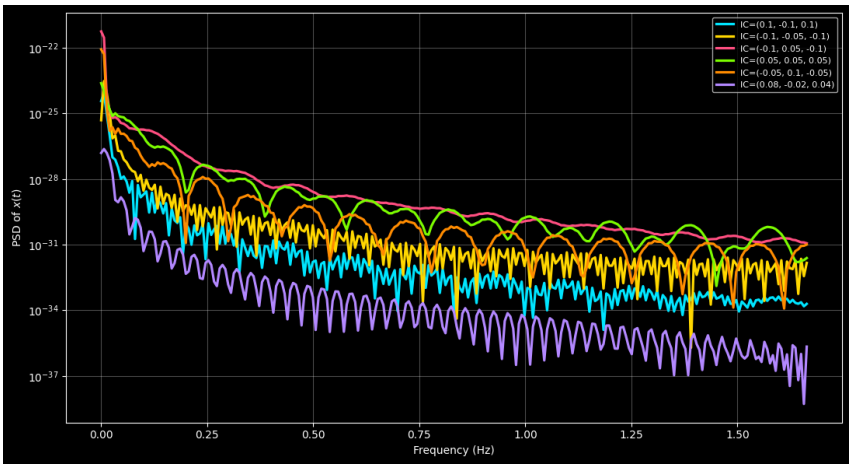

(a) For $p = -1.00$, $q = 0.20$

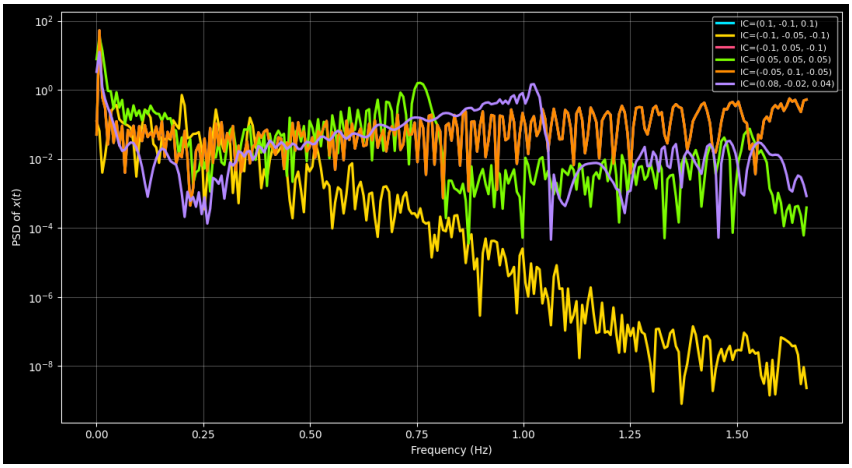

(b) For $p = -0.10$, $q = -0.10$

Figure 5. Power spectral analysis of the state variable $x(t)$ for multiple initial conditions.

Figure 5(b) illustrated the PSD of $x(t)$ under the same initial conditions, but in an alternate regimen of parameters, which shows a much more enriched spectral structure. Compared with Figure 5(a), the spectrum displays strong frequency-dependent modulations and sharp peaks, which means that there are favored frequency bands and the energy is concentrated in the system on them. The difference between the amplitudes of the various peaks and the spectral shapes of various initial conditions is

another evidence of the existence of multiple dynamical responses in the same parameter space, which highlights the nonlinear and sensitive behavior of the system in the frequency domain.

4. Statistical analysis

This section provides a detailed statistical analysis to explore the behavior of the system under different conditions. In this section, the systematic classification of the parametric space is presented to distinguish between behavior. This is then followed by KDE, which is used to describe probabilistic distributions, and an analysis of its sensitivity to the number of initial conditions. KDE-based statistical measures and an ensemble sensitivity analysis based on empirical CDFs are used, respectively, to provide a quantitative measure of temporal dynamics and uncertainty, respectively.

4.1. Systematic parametric space analysis of the RF system

To study the multidimensional behavior of the RF system described by our model equations (2.1), we developed a systematic two-dimensional parameter space of the control pair (p, q) to study its behavior in a structured way. Here, the parameters p and q can be treated as independent variables that range in the interval $[-1, 1]$, and both intervals are discretized into a finite set of values with equal space. This creates a geometric grid of the parameter space (p, q) that spans the selected space and gives a fine sampling of the possible configurations of the system. At each point on this grid, the system is run after a set of initial conditions with $x(0)$, $y(0)$, and $z(0)$ in $[-0.1, 0.1]$, with a fixed step size $h = 0.3$ in the case of a grid of initial conditions. This leads to the classification of the resulting trajectories based on statistical properties into stable, oscillatory, or unstable behaviors, under a diversity of initial conditions, to measure robustness. This multi-initial-condition approach shows the dynamical regimes and transitions that cannot be revealed through the individual trajectory. The graphical representation in Figure 6 shows that the search space is used for systematic parametric analysis.

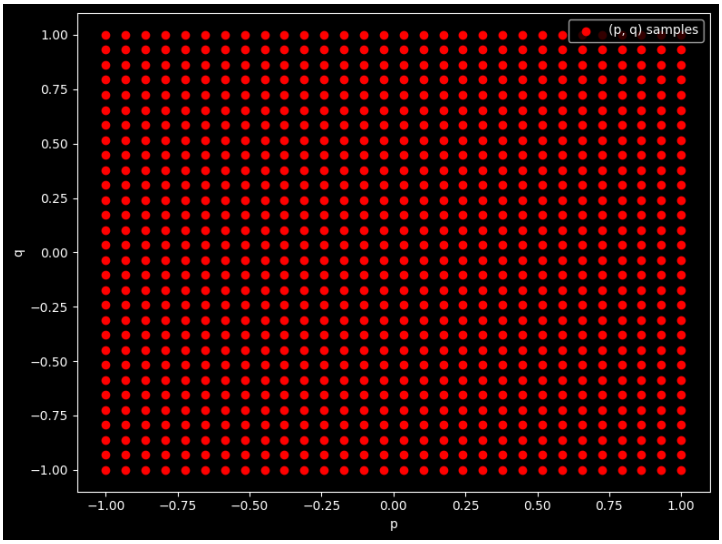

Figure 6. Search space in the (p, q) plane used for the systematic parametric analysis. Each point represents one parameter pair (p, q) with $p, q \in [-1, 1]$, at which the system is simulated from initial conditions $x(0)$, $y(0)$, and $z(0)$ taken in $[-0.1, 0.1]$.

4.1.1. Statistical mapping of the (p, q) parameter space

In this section, the statistical mapping of the (p, q) parameter space is performed to characterize the global dynamical behavior of an RF system under systematic parameter variations and various initial conditions.

The dynamical regimes in the parameter-space maps are classified according to the value of Δ_{overall}. A parameter point is said to be stable when $\Delta_{\text{overall}} < 0.5$, periodic when $0.5 \leq \Delta_{\text{overall}} \leq 10$, and unstable when $\Delta_{\text{overall}} > 10$. Each pair of parameters (p, q) is classified according to the trajectory resulting from the chosen initial condition, which is determined by numerical simulation. The corresponding colors in the parameter-space maps shown in Figure 7 represent the assignment of these parameters using established criteria.

The thresholds identified in this study were determined empirically based on a large number of numerical simulations. They were chosen because they provide a clear distinction between confined, bounded oscillatory trajectories and strongly divergent trajectories in the explored parameter space. To assess the numerical robustness of these thresholds, additional simulations were performed using different integration times and step sizes. The results indicate that, while there may be some minor quantitative variations, the qualitative classification of the dynamical regimes and the structure of the parameter-space maps remain consistent. This confirms that the adopted thresholds provide a reproducible and reliable characterization of the system dynamics. The parametric map of the dynamics of the system in the (p, q) plane is presented in Figure 7(a) with the initial condition $(-0.10, 0.00, 0.05)$. The map shows that there is a complicated distribution of stable, periodic, and unstable regions, which denotes that there are several dynamical behaviors. The irregular change of patterns indicates that the long-term response of the system is conditional on the initial state chosen in some combinations of parameters. A more simplified and organized parametric map is observed in Figure 7(b). The entire upper half of the behavior of the (p, q) plane is stable and the entire behavior of the bottom is unstable, creating an almost straight horizontal line between stability and instability. This distinct separation is an indication that the parameter q is the most significant in determining the behavior of the system in this initial state.

The parametric map once again depicts a complicated relationship between stability and instability, but the structure is now quite different, as observed in Figure 7(c). The stability of the (p, q) plane means that this region is always able to accommodate convergent behavior among various initial states. However, the parameter space contains most of the parameter space that is dominated by instability, showing that the system is prone to divergence over a wide range of parameter combinations. There is actually a very clearly noticeable segment of periodic dynamics at the border between the stable and unstable parts, which creates a thin transition zone. This initial condition is the one that generates the widest range in the unstable region, and indicates that the most common kind of response is instability and that periodic behavior is infrequent and highly sensitive to initial conditions and the choice of parameter.

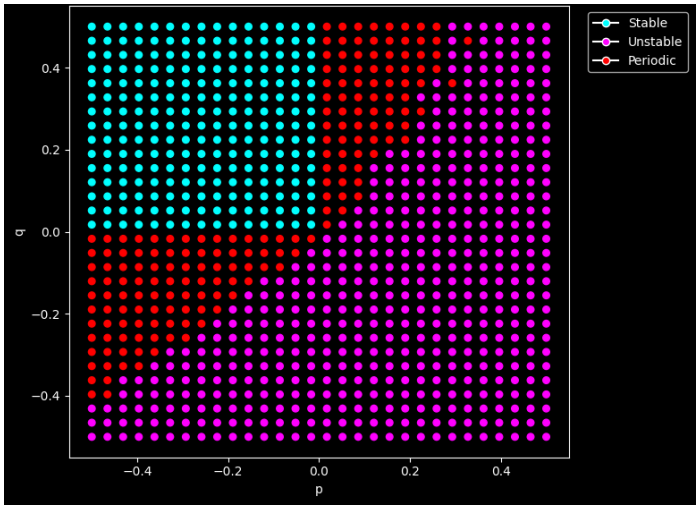

(a) For IC $(-0.10, 0.00, 0.05)$

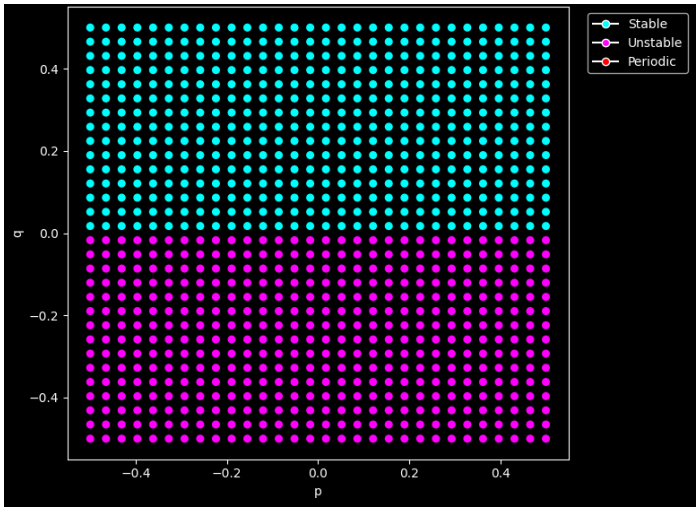

(b) For IC (0.00, 0.00, -0.05)

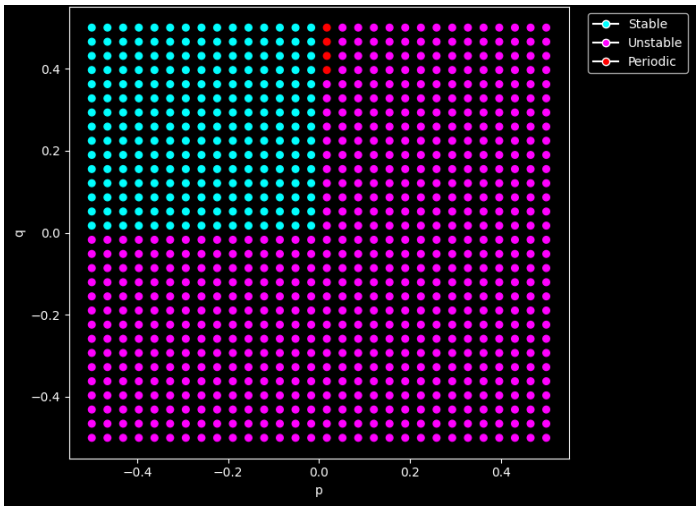

(c) For IC (0.05, 0.10, -0.10)

Figure 7. Parametric maps of system dynamics in the (p, q) plane for three different initial conditions.

4.2. KDE of the dynamical responses

In this section, KDE is used for the ensemble analysis data to investigate the distribution pattern and variability of the system response at different control parameters. The results of the KDE analysis are shown in Figure 8. The maximum excursion of trajectories in phase space is represented by the observed value of the logarithm, specifically $\log_{10}(r_{\max} + 1)$. Using a logarithmic scale helps compress the wide dynamic range of values for $r_{\max}$. This approach ensures that extreme values do not dominate the distribution and prevents outliers from skewing the results.

The KDE histogram of the observable $\log_{10}(r_{\max} + 1)$ calculated using an ensemble of trajectories of the initial conditions randomly sampled is shown in Figure 8(a). The distribution is concentrated and unimodal, with almost all sampled values clustering in a small range (indistinctly between 0.02 and 0.06). The KDE curve has one continuous peak, which means that most initial conditions have magnitudes similar to the initial trajectories in the phase space. The even distribution of KDE and its high accuracy similar to the histogram demonstrate that the distribution is stable and not controlled by outliers.

Figure 8(b) indicates a qualitatively different statistical structure of $\log_{10}(r_{\max} + 1)$. The histogram is no longer clumped about one small range; the values are strongly separated into values in a number of distinct regions, with a large concentration around and including very small values, and further concentration around much larger values (as indicated by the bars far to the right). This trend shows that the space of initial conditions results in high variability of the maximum excursion measure; there is no uniform behavior of the trajectories in terms of the largest radius.

Significant dispersion in $\log_{10}(r_{\max} + 1)$ persists in Figure 8(c), with the corresponding histogram once again showing values in separate areas and not within a single compact cluster. The KDE curve shows an evident multi-modal structure, i.e., the interactions of the trajectories give rise to multiple statistically independent results of the maximum radius measure. The high concentration of small values indicates that there are certain initial conditions that produce trajectories that are not very large during the integration period. In the meantime, having the additional density at very large values suggests that there are other initial conditions associated with ending up in trajectories with very large excursions in phase space. In practice, it implies that the response of the system is very sensitive to initial conditions in the sense that even minor variations in the starting points can produce values of $r_{\max}$ that are appreciably different.

These statistical patterns provide insight into the internal structure of phase space. A small unimodal KDE distribution represents a trajectory moving toward the largest attractor. In contrast, wider or multimodal distributions suggest multiple dynamical pathways and indicate historical sensitivity to initial conditions. Thus, KDE analysis offers a statistical perspective on how fluctuations in initial conditions influence the accessible areas of phase space.

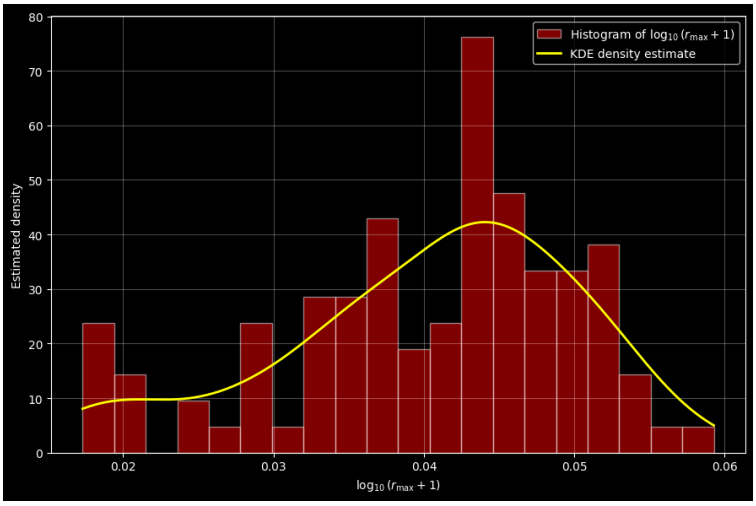

(a) For $p = -1.00$, $q = 0.20$

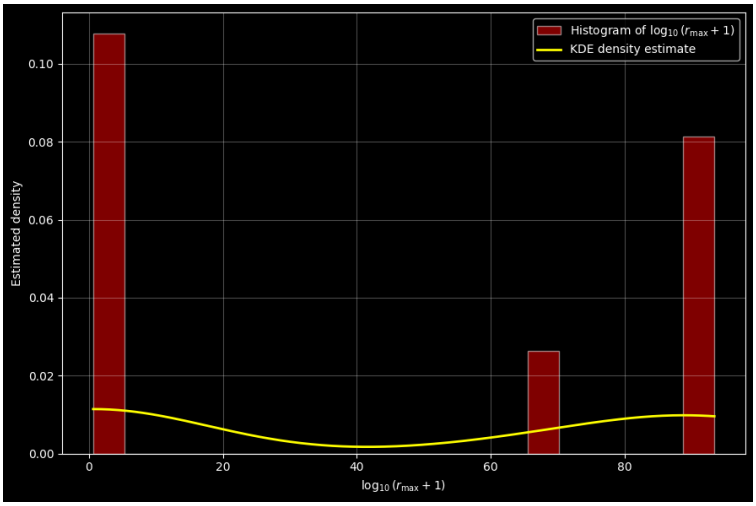

(b) For $p = -0.70$, $q = -0.10$

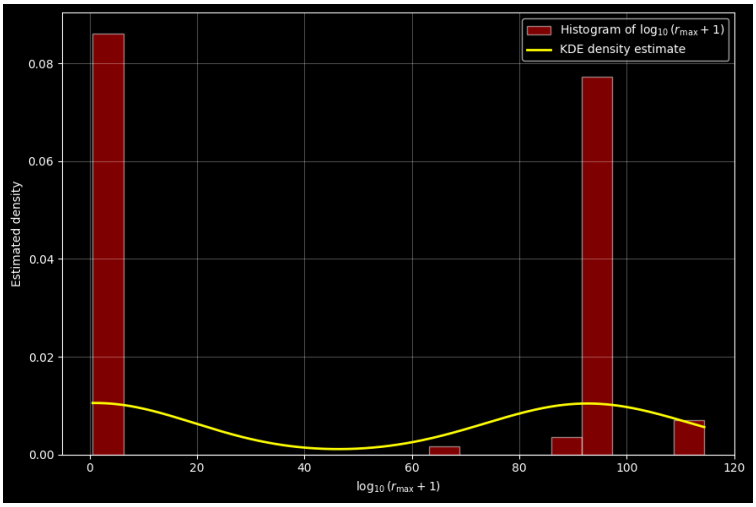

(c) For $p = -0.10$, $q = -0.10$

Figure 8. Observed distributional trends of the scalar observable $\log_{10}(r_{\max} + 1)$ for selected parameter sets.

4.3. Sensitivity of KDE to the number of initial conditions

In this section, the sensitivity of the KDE results to the number of initial conditions for a set of fixed system parameters is explored by increasing the size of the ensemble N. The parameter N is the size of the randomly sampled set of initial conditions with which the ensemble of trajectories is generated, and the higher the N, the more accurate the statistical description of the system response is possible. The KDE distributions of $\log_{10}(r_{\max} + 1)$ at various values of N were calculated and plotted in Figure 9 showing how the size of the ensemble influences the estimated probability density. Table 5 shows the average and standard error of observable $\log_{10}(r_{\max} + 1)$ in increasing the size of the ensemble N, calculated to measure the convergence and statistical power of the statistical characterization based on KDE in various parameters.

The KDE distributions corresponding to the parameter values $p = -0.70$ and $q = -0.10$ are displayed in Figure 9(a). In smaller ensemble sizes, the trend is similar, with significant differences in the density being found in the tails of the distribution, and this is sensitive to small sampling of the initial conditions. The growth of the size of the ensemble results in successively smoother KDE curves that tend to a steady shape. This persistence of a wide distribution indicates that the system is highly variable in its long response history, whereas the fact that the KDE curves approach the N large distribution indicates the soundness of the statistical description.

For parameter values $p = -1.00$ and $q = 0.20$, the resulting behavior is illustrated in Figure 9(b). Here, the KDE distributions are concentrated with a mostly unimodal structure in all sizes of ensembles. The main idea of increasing the number of initial conditions is to make the estimated density smooth without materially changing its qualitative form. This means that the parameter regime is less sensitive to initial conditions and that, with relatively small ensembles, it is possible to characterize it statistically with high reliability.

These observations also reflect differences in the underlying phase space organization. The parameter regimes that result in large-scale or multi-peaked KDE structures correspond to trajectories in phase space that explore more than one region and become increasingly sensitive to initial conditions. Unimodal and stable KDE profiles, on the other hand, are indicative of a dominant attractor.

Table 5. Statistical measures of $\log_{10}(r_{\max} + 1)$ for different ensemble sizes N.

Parameter set: $p = -0.70,\ q = -0.10$		
N	Mean	Standard Deviation
50	46.6018	41.6541
100	44.4905	43.5639
200	42.7190	43.4587
500	44.1747	43.2983
Parameter set: $p = -1.00,\ q = 0.20$		
N	Mean	Standard Deviation
50	0.0371	0.0122
100	0.0403	0.0098
200	0.0398	0.0100
500	0.0400	0.0113

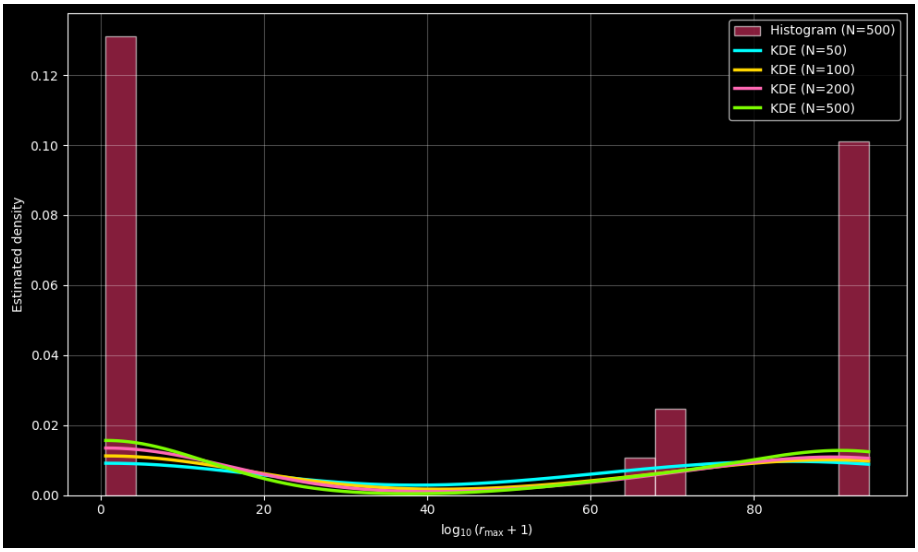

(a) For $p = -0.70$, $q = -0.10$

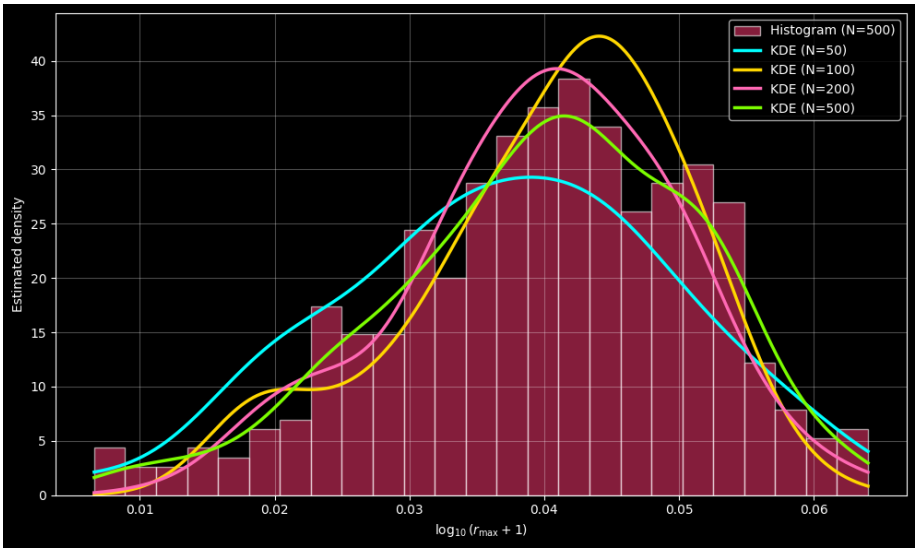

(b) For $p = -1.00$, $q = 0.20$

Figure 9. Sensitivity of the KDE distributions of $\log_{10}(r_{\max} + 1)$ to the number of initial conditions N.

4.4. Time-series dynamics with KDE-based statistical characterization

Time-domain analysis is explored along with KDE-based ensemble statistics to define a direct distribution between the behavior of individual trajectories and the statistical variability of the system (2.1). Figure 10 shows a joint analysis of the dynamic-time behavior, as well as the statistical response of the dynamical system in various parameter settings. The left panels of Figure 10 demonstrate how the state variables change over time given a single representative initial condition, which gives some idea of the qualitative dynamics of the system. The right panels of Figure 10 show the KDE of the observable scalar $\log_{10}(r_{\max} + 1)$ that is computed on an ensemble of randomly distributed initial conditions, thus representing the statistical variability of the response of the system. It is this

combined representation which is then used to directly give a relationship between the qualitative behavior of individual trajectories and the statistical variability of an ensemble based on the system in which the object is to undertake an evaluation of its sensitivity to initial conditions and variations of its parameters.

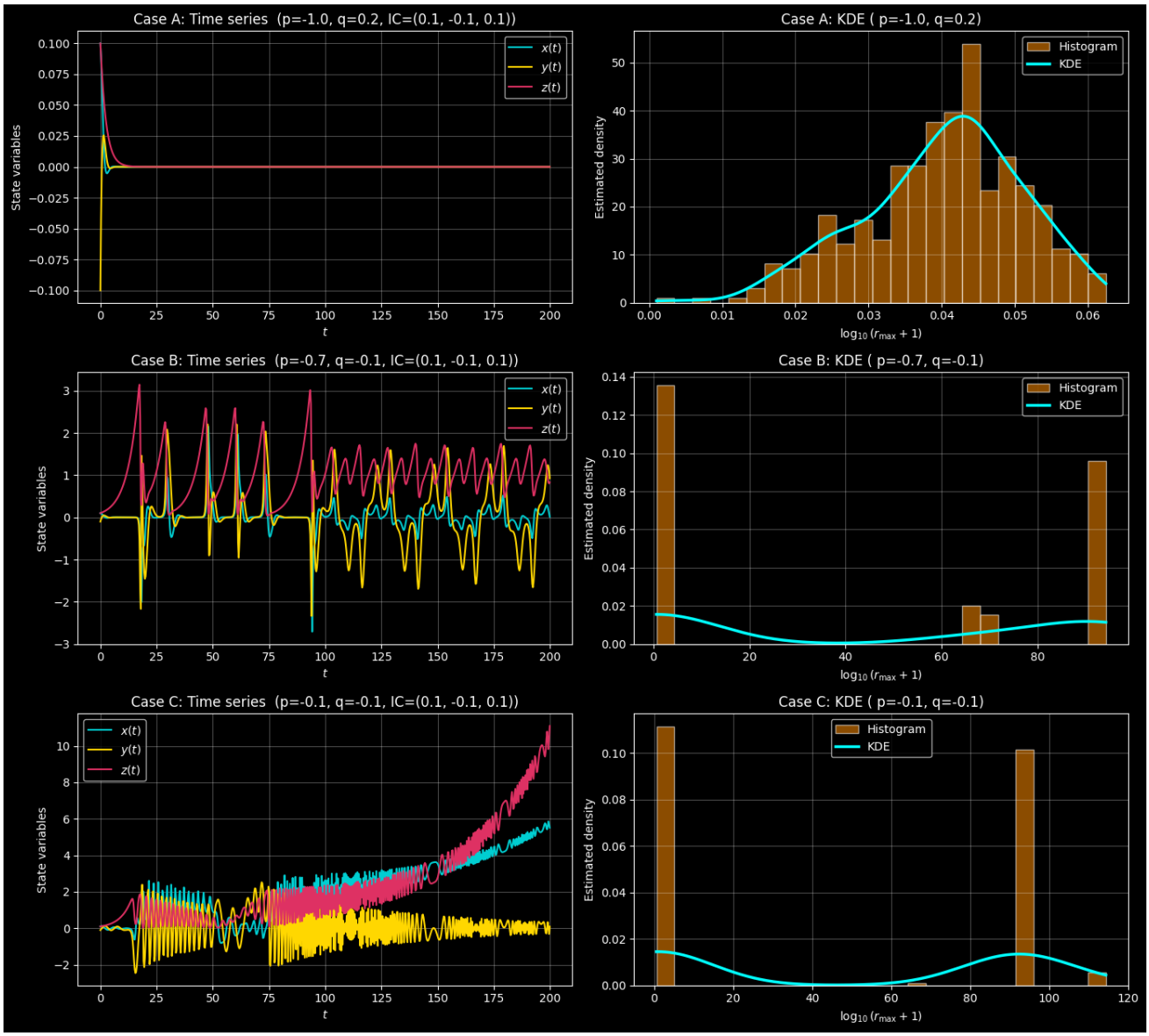

Figure 10. Combined visualization of time-series dynamics and KDE-based ensemble statistics. The left panels show a representative trajectory, while the right panels illustrate ensemble variability through KDE distributions, which may not be captured by a single trajectory.

In Case A ($p = -1.0$, $q = 0.2$), time-series trajectories quickly go to zero, which means a strong damping effect and recovery to the stable point. This routine is manifested in the respective KDE plot, which demonstrates a skinny single-mode distribution, indicating insignificant sensitivity to changes in initial situations.

However, Case B ($p = -0.7$, $q = -0.1$) exhibits long-term fluctuations that have nonlinear oscillating dynamics with intermittent amplitude in the time sequence. The related KDE distribution is much more dispersed, meaning better variability and sensitivity to initial conditions within the ensemble.

In Case C ($p = -0.1$, $q = -0.1$), the time-series development is clearly seen to increase in amplitudes and with irregular behavior, which is typical of an unstable or strongly nonlinear regime. The KDE plot of this case is a wide and distributed distribution with a high sensitivity and great variation of the response of the system. Table 6 provides the behavior of the time series and compares the related statistical features based on KDE of the analyzed cases.

Table 6. Comparison of time-series behavior and KDE-based statistical characteristics.

Case	Parameters (p, q)	Time-series behavior	KDE distribution
A	$(-1.0,\ 0.2)$	Rapid decay to equilibrium	Narrow, unimodal
B	$(-0.7,\ -0.1)$	Sustained irregular oscillations	Broad distribution
C	$(-0.1,\ -0.1)$	Growing / irregular amplitudes	Very broad distribution

4.5. Ensemble sensitivity analysis using empirical CDFs

This section examines the sensitivity of the ensemble using empirical CDFs to study the distribution of $r_{\max}$ as the ensemble size increases, with other combinations of parameters. Figure 11 shows CDF comparisons of four combinations of parameters. The combinations of parameters (p, q) that are used in this section are listed in Table 7.

Table 7. Parameter sets (p, q) used in the CDF convergence analysis.

Sets	Parameter Values (p, q)
Set A	$(p, q) = (-1.0, -0.4)$
Set B	$(p, q) = (-1.0, 0.2)$
Set C	$(p, q) = (-1.0, 0.8)$
Set D	$(p, q) = (-0.7, -0.4)$

In the parameter sets $(p, q) = (-1.0, -0.4)$ and $(p, q) = (-1.0, 0.2)$, the empirical CDFs show different effects of the ensemble size. In the former case, CDFs for various ensemble sizes lie near a single curve, a manifestation of rapid statistical convergence and low sensitivity to initial conditions. $N \in \{50, 100, 120, 150, 200\}$ are generated using a nested sampling strategy, taking into account that smaller ensembles are strict subsets of larger ones. The initial conditions used to build the ensembles are uniformly sampled within a defined initial-condition domain. A nested sampling strategy has been employed, where the larger ensemble includes all elements of the smaller ones. Specifically, $N = 50$ is a subset of $N = 100$, and similarly for $N = 120$, $N = 150$, and $N = 200$. This method ensures uniformity in the comparison of empirical CDFs and allows for systematic observation of convergence behavior as the size of the ensemble increases. This implies that the system dynamics in this regime are relatively uniform, and even smaller ensembles provide a good characterization. In contrast, in $(p, q) = (-1.0, 0.2)$, deviations are easily observed in small ensembles, especially in $N = 50$, and an increase in the size of an ensemble tends to converge.

For the parameter combinations $(p, q) = (-1.0, 0.8)$ and $(p, q) = (-0.7, -0.4)$, the CDFs are more diffuse and converge less slowly to the size of the ensemble. Such instances indicate a broader spread of transmission in the system's reaction, implying an expanded range of accessible dynamical behavior. Although convergence was eventually obtained for larger N, visible differences at smaller ensemble sizes indicate greater sensitivity to initial conditions relative to the initial parameter set. These outcomes are an expression of variations in the phase-space organization. Rapid convergence of the empirical CDF is associated with trajectories converging toward a shared dynamical region. In contrast, slow convergence is associated with multiple dynamical trajectories and greater sensitivity to initial conditions.

The observation of variations in the parameter sets shown in Figure 11 indicates differences in the underlying dynamical stability of the RF system. For example, the rapid convergence of the empirical CDFs in Set A suggests that, given a different set of initial conditions, the system would likely reach a similar dynamical region. This observation implies the existence of a structurally stable attractor. In contrast, the greater divergence between the CDF curves in Sets C and D indicates a more varied system response, resulting in multiple dynamical pathways. This behavior aligns with parameter regimes where stability is diminished, and the system is more susceptible to complex dynamical transitions, potentially linked to bifurcation-related shifts toward irregular or chaotic motion.

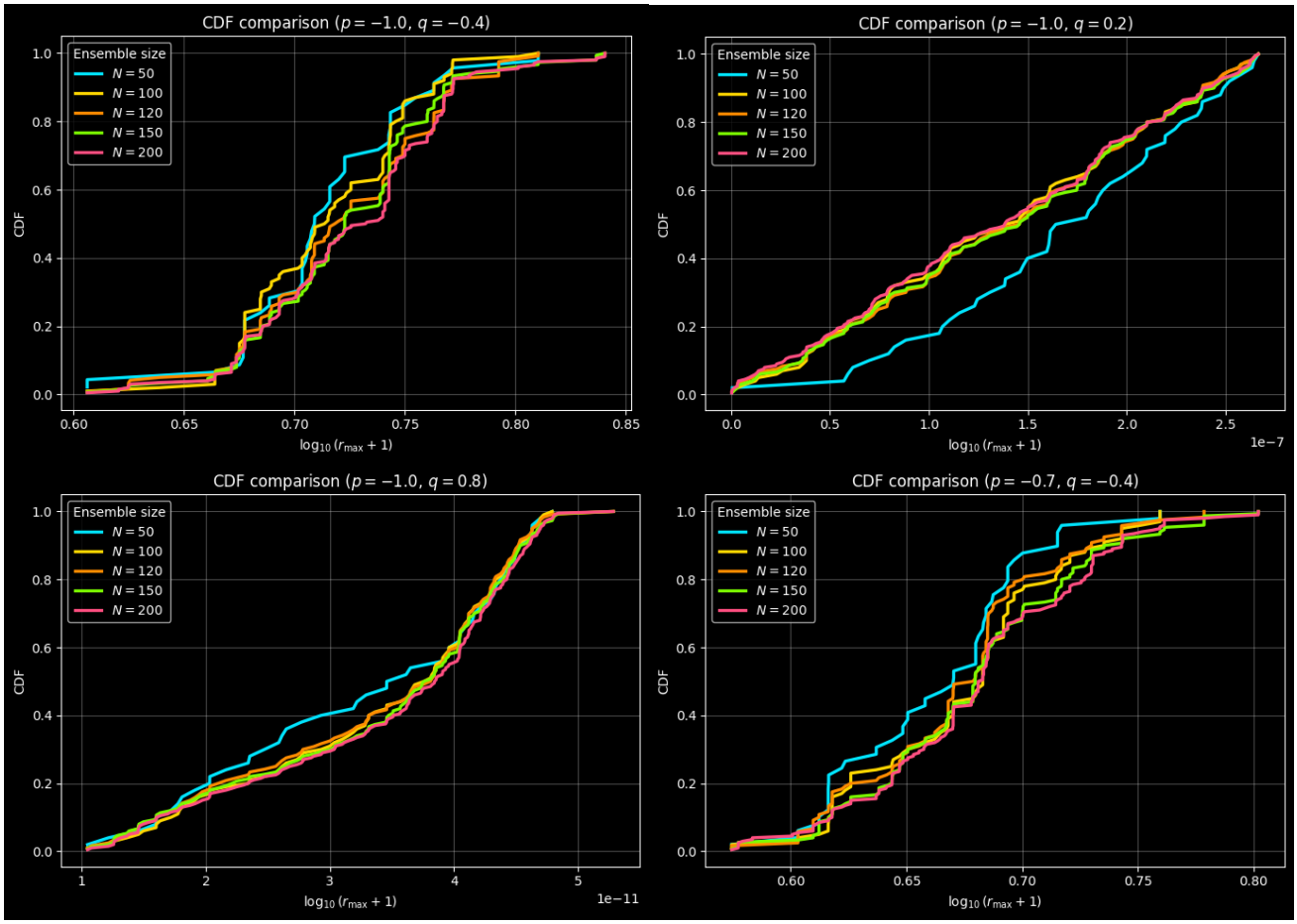

Figure 11. CDF comparison for selected parameter sets using nested initial conditions.

5. Conclusions

In this study, the RF system was methodically examined in the constrained control-parameter space $(p, q) \in [-1, 1] \times [-1, 1]$ using ensembles of initial conditions taken from $[-0.1, 0.1]$ for each state variable to provide a detailed characterization that goes beyond individual trajectories. In contrast to conventional analyses that focus on individual trajectory studies, the present research merges classical dynamical diagnostics with statistical characterization based on ensembles to provide a more comprehensive understanding of the system dynamics. The analysis was performed by integrating classical dynamical diagnostics, i.e., time-series evolution and power spectral density, with ensemble-based statistical indicators, i.e., KDE, empirical CDF, to identify clear areas of stable, periodic, and unstable behavior, sharp transitions, and statistically sensitive zones. These findings indicate that some parameter regimes are fast converging and highly robust to changes in initial conditions, and some are highly variable and slowly converging as an ensemble, and show the inherent multistability and sensitivity of the RF system. The resultant dynamical-statistical system offers an objective and quantitative mapping of the RF dynamical events through parameter space and offers a more reliable scheme of classification of system behavior and uncertainty than a simple trajectory-based analysis. This framework will be continued to finer parameter resolutions and larger ensembles in the future to resolve transitional regimes and rare dynamical events in a better way. The proposed methodology can be applied in real-life systems where robustness and sensitivity are critical. In engineering systems, such as nonlinear circuits, it can assist the stability and performance analysis of systems under uncertain conditions, whereas in biological and physiological systems, it may aid in the quantification of variability and transitions in complex dynamical signals. In addition, the procedure can be extended to establish the uncertain propagation and robustness of the RF system in higher dimensions or with perturbed forces in order to determine uncertainty propagation in stochastically perturbed systems.

Author contributions

H. Sajjad: Visualization, methodology, writing – original draft preparation; A. Jhangeer: Conceptualization, visualization, methodology, supervision, writing – reviewing and editing, investigation; M. Imran: Writing – reviewing and editing, funding acquisition, validation; A. R. Ansari: Visualization, methodology, software, supervision. All authors have read and approved the final version of the manuscript for publication.

Use of Generative-AI tools declaration

The authors declare they have not used Artificial Intelligence (AI) tools in the creation of this article.

Acknowledgments

M. Imran would like to express his sincere gratitude to Ajman University for the financial support and resources provided for this research under the Internal Research Grant No. DRG Ref. Number: 2025-IRG-CHS-17. This article has been produced with the financial support of the European Union under the REFRESH – Research Excellence For Region Sustainability and High-tech Industries project

number CZ .10.03.01/00/22_003/0000048 via the Operational Programme Just Transition.

Conflict of interest

All authors declare no conflicts of interest in this paper.

References

1. S. H. Strogatz, *Nonlinear dynamics and chaos: With applications to physics, biology, chemistry, and engineering*, Chapman and Hall/CRC, 2024.
2. L. H. Monteiro, *Overview of dynamical systems and chaos*, in: Chaotic signals in digital communications, CRC Press, 2018, 83–110. https://doi.org/10.1201/9781315216256-3
3. J. M. Amigó, F. Montani, Nonlinear dynamics and applications, *Entropy*, **27** (2025), 688. https://doi.org/10.3390/e27070688
4. S. Banerjee, L. Rondoni, M. Mitra, *Applications of chaos and nonlinear dynamics in science and engineering*, Springer, 2012.
5. B. Hasselblatt, A. Katok, A. B. Katok, *Introduction to the modern theory of dynamical systems*, Cambridge University Press, 1995.
6. R. P. Agarwal, *Dynamical systems and applications*, World Scientific, 1995.
7. G. Litak, Chaotic vibrations in a regenerative cutting process, *Chaos Soliton. Fract.*, **13** (2002), 1531–1535. https://doi.org/10.1016/S0960-0779(01)00176-X
8. M. Watanabe, A. Prasad, K. Sakai, Delayed feedback active suspension control for chaos in quarter car model, *Chaos Soliton. Fract.*, **186** (2024), 115236. https://doi.org/10.1016/j.chaos.2024.115236
9. D. Feng, A compactor-soil coupling model considering mechanical inertia, *Int. J. Nonlin. Mech.*, **179** (2025), 105245. https://doi.org/10.1016/j.ijnonlinmec.2025.105245
10. V. In, P. Longhini, A. Palacios, *Applications of nonlinear dynamics*, Springer, 2008.
11. J. Awrejcewicz, *Applied non-linear dynamical systems*, Springer, 2014.
12. S. Leng, W. Lin, J. Kurths, Basin stability in delayed dynamics, *Sci. Rep.*, **6** (2016), 21449. https://doi.org/10.1038/srep21449
13. R. Dilão, *Dynamical system and chaos: An introduction with applications*, Springer, 2023. https://doi.org/10.1007/978-3-031-25154-2
14. Y. A. Madani, K. Aldwoah, B. Younis, M. Alsharafi, O. Osman, B. Muflh, Analysis and secure communication applications of a 4D chaotic system, *Sci. Rep.*, **15** (2025), 14104. https://doi.org/10.1038/s41598-025-98807-1
15. P. Kakou, S. K. Gupta, O. Barry, A nonlinear analysis of a Duffing oscillator, *Nonlinear Dynam.*, **112** (2024), 5847–5862. https://doi.org/10.1007/s11071-023-09163-6
16. D. N. Butusov, D. O. Pesterev, A. V. Tutueva, D. I. Kaplun, E. G. Nepomuceno, New technique to quantify chaotic dynamics, *Commun. Nonlinear Sci.*, **92** (2021), 105467. https://doi.org/10.1016/j.cnsns.2020.105467

17. M. R. Sales, M. Mugnaine, E. D. Leonel, I. L. Caldas, J. D. Szezech, Shrinking shrimp-shaped domains and multistability, *Chaos*, **34** (2024). https://doi.org/10.1063/5.0233324

18. M. I. Rabinovich, A. L. Fabrikant, Stochastic self-modulation of waves in nonequilibrium media, *J. Exp. Theor. Phys*, **77** (1979), 617–629.

19. M. F. Danca, P. Bourke, N. Kuznetsov, Graphical structure of attraction basins, *Int. J. Bifurcat. Chaos*, **29** (2019), 1930001. https://doi.org/10.1142/S0218127419300015

20. A. P. Kuznetsov, S. P. Kuznetsov, L. V. Turukina, Complex dynamics in the Rabinovich-Fabrikant model, *Izv. Sarat. Univ.*, **19** (2019), 4–18.

21. M. F. Danca, N. Kuznetsov, G. Chen, Unusual dynamics and hidden attractors, *Nonlinear Dynam.*, **88** (2017), 791–805. https://doi.org/10.1007/s11071-016-3276-1

22. M. F. Danca, Hidden transient chaotic attractors, *Nonlinear Dynam.*, **86** (2016), 1263–1270. https://doi.org/10.1007/s11071-016-2962-3

23. S. P. Kuznetsov, L. V. Turukina, Generalized Rabinovich-Fabrikant system, *Appl. Nonlinear Dyn.*, **30** (2022), 7–29. https://doi.org/10.18500/0869-6632-2022-30-1-7-29

24. M. F. Danca, N. Kuznetsov, Hidden strange nonchaotic attractors, *Mathematics*, **9** (2021), 652. https://doi.org/10.3390/math9060652

25. G. E. Arif, A. T. Ahmad, Analysis of novel 4D Rabinovich-Fabrikant system, *Eur. J. Pure Appl. Math.*, **16** (2023), 1991–2004. https://doi.org/10.29020/nybg.ejpam.v16i3.4857

26. C. Alvares, S. Banerjee, Probabilistic distance-based stability quantifier, *Nonlinear Dynam.*, **112** (2024), 21869–21880. https://doi.org/10.1007/s11071-024-10176-y

27. A. A. Popov, E. M. Zucchelli, R. Zanetti, Kernel density estimation with applications, *Comput. Geosci.*, **29** (2025), 1–23. https://doi.org/10.1007/s10596-025-10354-w

28. U. Feudel, Complex dynamics in multistable systems, *Int. J. Bifurcat. Chaos*, **18** (2008), 1607–1626. https://doi.org/10.1142/S0218127408021233

29. P. J. Menck, J. Heitzig, N. Marwan, J. Kurths, Basin stability complements linear stability, *Nat. Phys.*, **9** (2013), 89–92. https://doi.org/10.1038/nphys2516

30. P. Brzeski, M. Lazarek, T. Kapitaniak, J. Kurths, P. Perlikowski, Basin stability approach for multistable systems, *Meccanica*, **51** (2016), 2713–2726. https://doi.org/10.1007/s11012-016-0534-8

31. V. S. Anishchenko, T. E. Vadivasova, G. A. Okrokvertskhov, G. I. Strelkova, Statistical properties of dynamical chaos, *Phys. Usp.*, **48** (2005), 151. https://doi.org/10.1070/PU2005v048n02ABEH002070

32. S. Galatolo, I. Nisoli, C. Rojas, Probability and computation in dynamical systems, *Math. Struct. Comput. Sci.*, **24** (2014).

33. V. Baladi, *Spectrum and statistical properties of chaotic dynamics*, in: European Congress of Mathematics, 2001, 203–223. https://doi.org/10.1007/978-3-0348-8268-2_11

34. R. Varga, K. Klapcsik, F. Hegedüs, Route to shrimps, *Chaos Soliton. Fract.*, **130** (2020), 109424. https://doi.org/10.1016/j.chaos.2019.109424

35. D. F. M. Oliveira, Mapping chaos in Ikeda map, *Chaos*, **34** (2024).

36. S. A. Hassan, M. J. A. A. Raja, S. Z. A. Sherazi, C. Y. Chang, C. M. Shu, A. K. Kiani, et al., Predictive analysis of fractional-order chaotic attractors, *Nonlinear Dynam.*, 2025, 1–33.
37. V. S. H. Rao, N. Yadaiah, Parameter identification of dynamical systems, *Chaos Soliton. Fract.*, **23** (2005), 1137–1151. https://doi.org/10.1016/j.chaos.2003.09.047
38. Y. Zou, R. V. Donner, N. Marwan, J. F. Donges, J. Kurths, Complex network approaches to nonlinear time series, *Phys. Rep.*, **787** (2019), 1–97.
39. M. H. Same, G. Gandubert, G. Gleeton, P. Ivanov, R. Landry Jr, Simplified Welch algorithm, *Appl. Sci.*, **11** (2020), 86.
40. L. Wasserman, *All of nonparametric statistics*, Springer, 2006.
41. Z. Wang, D. W. Scott, Nonparametric density estimation, *WIRES Water*, **11** (2019), e1461.
42. D. W. Scott, *Multivariate density estimation: Theory, practice, and visualization*, Wiley, 2015.
43. G. Casella, R. Berger, *Statistical inference*, Chapman and Hall/CRC, 2024.

AIMS Press